Check for updates

Enhanced removal of fluoride by zirconium modified tea waste with extrusion treatment: kinetics and mechanism†

Liping Mei, [iD] ‡ Chuanyi Peng,‡ Huanhuan Qiao, Fei Ke, Jin Liang, Ruyan Hou, Xiaochun Wan* and Huimei Cai*

To improve the adsorption efficiency of tea-based biosorbents for removing fluoride in drinking water, the novel and effective adsorbent was formed by treating tea waste with extrusion technology. In this study, the extrusion technology was applied to the preparation of adsorbents for the first time. A low-priced and more efficient adsorbent was prepared by loading zirconium onto extruded tea waste (EXT-Zr). Extruded tea waste increased the surface pore size, which could provide more loading sites for zirconium. The EXT-Zr effectively removed fluoride from water in a pH range of 3.0–10.0, which is wider than the pH range of zirconium-loaded tea waste (Tea-Zr). The adsorption was fitted by a pseudo-second order kinetic model and the Langmuir adsorption model. The maximum adsorption capacity was 20.56 mg g^{-1}. The EXT-Zr adsorbent was characterized by Scanning electron microscopy (SEM), Energy-Dispersive Spectroscopy (EDS), X-ray diffraction (XRD), a Brunauer–Emmett–Teller (BET) method, Fourier-transform infrared (FTIR) and X-ray photoelectron spectroscopy (XPS) to prove the mechanism of how EXT-Zr adsorbs fluoride. The results proved that EXT-based adsorbent will be effective for the enhanced removal of fluoride in drinking water.

1. Introduction

Fluoride is a widespread element found mainly in nature.[1] Fluoride is considered as an essential trace element for human beings[2] and can prevent dental caries by reducing the demineralization rate of enamel or by increasing the rate of remineralization.[3] Although fluoride is beneficial, excess fluoride can lead to multifarious diseases, such as arthritis, skeletal fluorosis, infertility, osteoporosis and so on.[4,5] Due to the hazards of excessive fluoride, the World Health Organization (WHO) has stipulated a limit of fluoride in drinking water (1.5 mg L^{-1}).[6]

Fluoride pollution of drinking water has been recognized as a public health risk in most of the world.[7] Fluoride in water is caused by pollution with industrial wastewater and by geochemical weathering of rocks, for example, fluorapatite, which is the main source of fluoride toxicity. Groundwater resources in China, India and some western countries (such as the United States and Mexico) contain high concentrations of fluoride.[8] Therefore, it is significant to decrease the fluoride content in water prepared for drinking by the public.

There are a few methods to remove fluoride, including coagulation/precipitation methods,[9] ion-exchange processes,[10] membrane processes,[7] and adsorption processes.[11] Each technique has advantages and limitations, including the conditions under which it performs the best. Adsorption technology is widely used, because of its safety, simplicity, inexpensive, and high efficiency.[12] The adsorbent materials most generally utilized for defluoridation include activated alumina,[13] activated carbon,[8] bone char[14] and zeolites.[15] More and more people use biopolymers as adsorbent materials because of their nontoxicity, good biocompatibility, and low cost. Biopolymer materials are usually modified with metals (iron, aluminum, *etc.*) such as pectin,[16] alginate,[17] cellulose,[18] chitosan,[19] *etc.* However, these absorbents have several disadvantages, such as difficulty in handling and a narrow pH range for effective adsorption.[20] Therefore, it is meaningful to synthesize an effective and low-priced adsorbent for fluoride removal.

To improve the adsorption performance of biological materials, many physical or chemical methods have been adopted, such as ball milling,[21] enzymatic hydrolysis,[22] and composite metal modification.[20] Extrusion technology is a thermal mechanical preprocessing method for materials, due to its low cost, controllable temperature and screw speed, high shear and excellent processing ability. Twin-screw extrusion is the main method at present. Compared with ball mill and homogenizer,

School of Tea & Food Science and Technology, Anhui Agricultural University, State Key Laboratory of Tea Plant Biology and Utilization, No. 130 Changjiangxi Road, Hefei 230036, Anhui, People's Republic of China. E-mail: hml20@sina.com; xcwan@ahau.edu.cn

‡ Liping Mei and Chuanyi Peng contributed equally to this work.

twin-screw extruder has higher solid phase load and lower energy consumption.[23] Twin-screw extrusion is a thermo-mechanical process, and the chemical and thermal properties of the extruded products are similar to those of the original biological materials because no compounds are removed.[24] Twin-screw extrusion technology may change the size of ligno-cellulose by increasing the surface area of lignocellulose, creating more pores and voids.[25] At present, twin-screw extrusion technology has been used to pretreat many kinds of lignocellulosic materials such as straw,[26] pineapple leaf,[27] bagasse[28] and corn stover.[29] However, twin-screw extrusion technology has not been applied to biosorbents so far.

In this study, a new adsorbent (EXT-Zr) was prepared by combining twin-screw extrusion of tea byproducts with the zirconium. The adsorption kinetics and adsorption isotherms were calculated, and the adsorbent dosage, solution pH, contact time, initial fluoride concentration and co-existing ions were varied in the starting reaction. The mechanism by which the adsorbent removed fluoride is proposed.

2.   Materials and methods

2.1.   Experimental materials

Spent tea leaves were gathered from a tea factory. Tea was washed with boiling, distilled water several times, until the washing liquid was colorless. The washed materials dried in a drying oven at 80 °C for 8 h and crushed, and were processed by an extruder (DSE32, twin-screw extruder, Jinan Shengrun Machinery Co., Ltd). After adjusting the moisture content of the materials to 30%, the extrusion was carried out, feeding speed was 12 Hz, and the temperature of the barrel zone 1 was 60 °C, the temperature of the barrel zone 2 was 135 °C, the tempera-ture of the barrel zone 3 was 140 °C, and the screw rotation speed was 35 Hz. After that, extruded tea waste (EXT) were ob-tained. The Tea and EXT were ground and sifted mesh 60. The Tea and EXT obtained were used in the following experiment to prepare composite biosorbents.

Chemical reagents used in this experiment were analytical grade (A.R.) and procured from Sinopharm Chemical Reagent Co., Ltd. (Shanghai, China).

2.2.   Preparation of biosorbent composites

A 0.4 mol L^{-1} Zr solution was made by mixing $ZrOCl_2 \cdot 8H_2O$ in distilled water. Tea (5 g) or EXT (5 g) was immersed in 100 mL of the Zr solution at 300 rpm at 60 °C for 1 h on a heated magnetic stirrer. Then, 2.0 mol L^{-1} NaOH was added dropwise to regulate the mixture pH to 7.0, kept stirring for 30 min. Finally, the mixture was centrifuged, washed a few times with distilled water, then dried in a drying oven at 70 °C for 10 h.

2.3.   Biosorbents characterization

Microscopic surface morphology and characteristics were detected by scanning electron microscopy (SEM, Sirion from FEI). Surface elements of the adsorbent were detected by Energy Dispersive Spectrometer (EDS, Sirion from FEI). The crystalline structure of the adsorbent was detected by X-ray diffraction

(XRD, X'Pert PRO from PHILIPS). The chemical bonding envi-ronments and adsorption sites were analyzed by X-ray photo-electron spectroscopy (XPS, Thermo Scientific Instrument Co. USA) Surface functional groups were detected by Fourier-Transform Infrared Spectroscopy (FTIR, Thermo Scientific Instrument Co. USA). The pore size distribution and surface area were detected by N_2 chemisorptions measurements with Brunauer–Emmett–Teller (BET) analysis.

2.4.   Batch adsorption experiment

Batch adsorption experiments were executed to determine the adsorption of fluoride on the adsorbents. The impacts of adsorbent dosage (0.5–2.0 g L^{-1}), solution pH (3–12), contact time (1–300 min), initial fluoride concentration (5–400 mg L^{-1}), and other co-existing anions (SO_4^{2-}, NO_3^-, Cl^-, and HCO_3^-) were examined. The initial solution pH was regulated with HCl and/or NaOH. Batch adsorption works were performed with 25 mL of fluoride solution in 50 mL centrifuge tubes at room temperature (25 °C). After the addition of the test dose of bio-sorbents into the fluoride solutions, the centrifuge tube was shaken at 300 rpm for 90 minutes on the shaker. After the above steps, the mixed solution was divided by filtration and the residual fluoride ion concentration was detected by ion selective electrode method.[21]

The removal efficiency (η) for the fluoride ions and the total fluoride adsorbed (mg g^{-1}) at equilibrium (q_e) were obtained from eqn (1) and (2).

$$\eta = \frac{C_0 - C_1}{C_0} \times 100\% \qquad (1)$$

$$q_e = \frac{V(C_0 - C_1)}{m} \qquad (2)$$

where η (%) represents the removal efficiency of the fluoride, C_0 represents the initial fluoride concentrations (mg L^{-1}) and C_1 represents the after-adsorption fluoride concentrations (mg L^{-1}), m represents the dry weight of the adsorbent (g), and V represents the volume of fluoride solution (mL). Each work was performed three times, and adsorption capacity was showed as the average ± standard deviation.

3.   Result and discussion

3.1.   Tea waste *versus* extruded tea waste

The surface topography of the Tea and EXT were observed by SEM. The surface of the Tea was smooth (Fig. 1a). The surface of the EXT was rough and had tiny pores (Fig. 1b and c). The surface areas of the Tea and EXT were 2.085 and 3.126 m² g^{-1}, respectively. The pore sizes were measured by BET, and the average pore radius was 0.44 nm in the Tea and 14.42 nm in the EXT (Fig. 2a). The pore diameter in the EXT much larger than in the Tea, and this increase is attributable to the extrusion process. These changes may increase the surface area and thus the adsorption capacity.

The defluoridation of Tea, EXT, Tea-Zr and EXT-Zr were compared in experiments using 0.030 g adsorbent and 25 mL 10 mg L^{-1} fluoride solution (Fig. 2b). Both the Tea and EXT
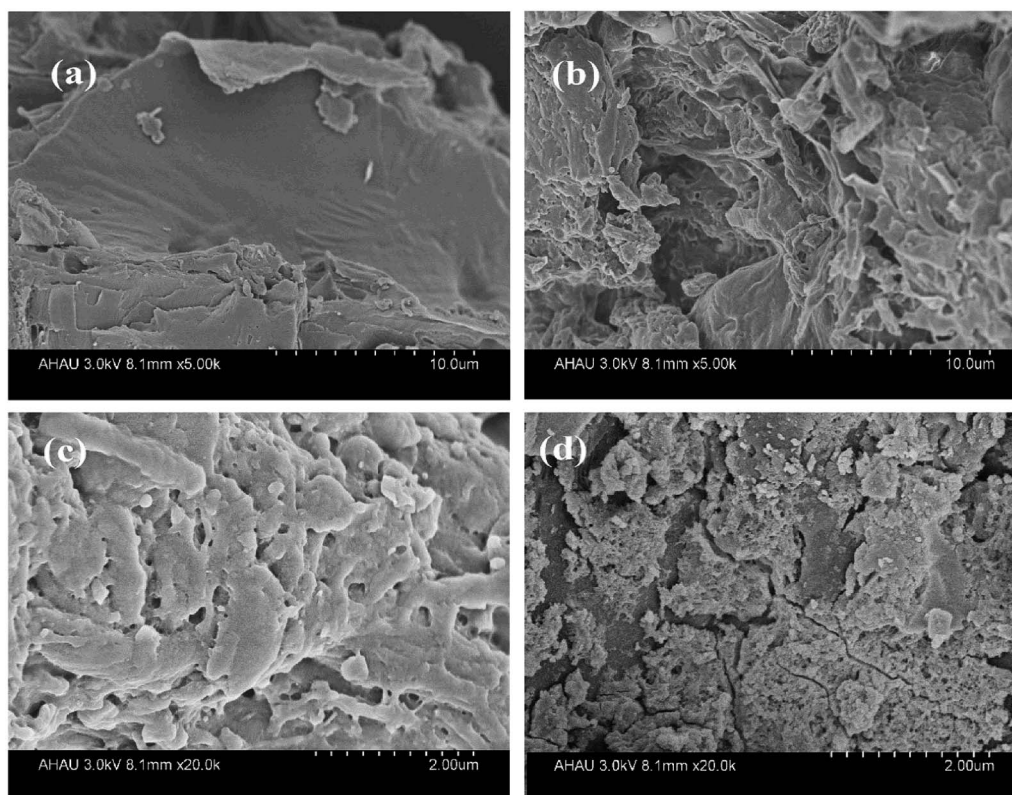
Fig. 1 SEM images of tea waste (a), extruded tea waste (EXT, b), at higher magnification (EXT, c) and extruded tea waste with zirconium (EXT-Zr, d).

adsorbents had extremely low fluoride adsorption efficiencies. The adsorption rate of Tea-Zr was 61%. The adsorption rate of EXT-Zr, using the extruded tea as the scaffold, reached 97%. Since the extrusion process increased the pore size, exposing a greater number of functional groups, the EXT was able to load more zirconium than the unextruded tea, thereby greatly improving the adsorption efficiency of fluoride.

3.2. Batch defluoridation experiment

3.2.1. Effect of adsorption dosage. The effect of the adsorbent dosage (for Tea-Zr and EXT-Zr) on fluoride removal is displayed in Fig. 3a. The adsorption doses ranged from 0.32 to 2 g L^{-1} while the other parameters remained constant, at a concentration of 10 mg L^{-1} fluoride in a solution of pH of 6.8 ± 0.3 and a contact time of 90 min. Increasing the EXT-Zr dose from 0.32 to 1.2 g L^{-1} rised the adsorption rate from 26% up to 97%. Perhaps this is because the increased dose of EXT-Zr will provide more active sites. After the amount of EXT-Zr adsorbent exceeded 1.2 g L^{-1}, the fluoride removal rate does not significantly increase, indicating that the reduce in the concentration of fluoride in the solution at these levels of adsorbent are so low that fluoride adsorption slows as fewer fluoride ions are available.[30] On the other hand, the sorbent made with unexpanded
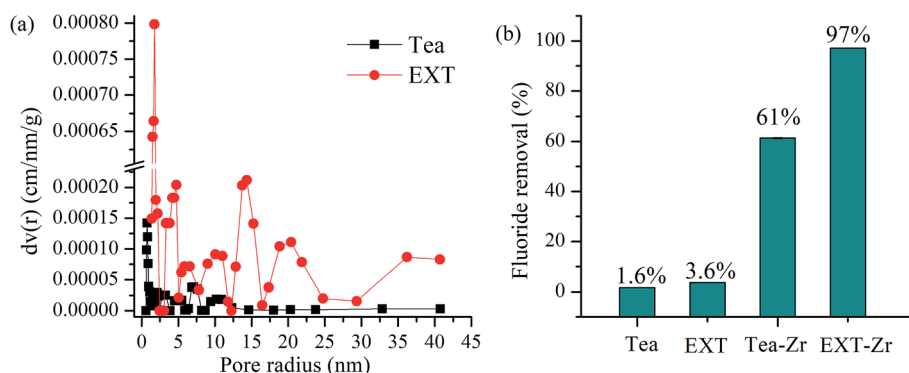

Fig. 2 Pore size distribution in Tea and EXT (a), comparison of the fluoride removal efficiencies of Tea, EXT, Tea-Zr, and EXT-Zr (b).
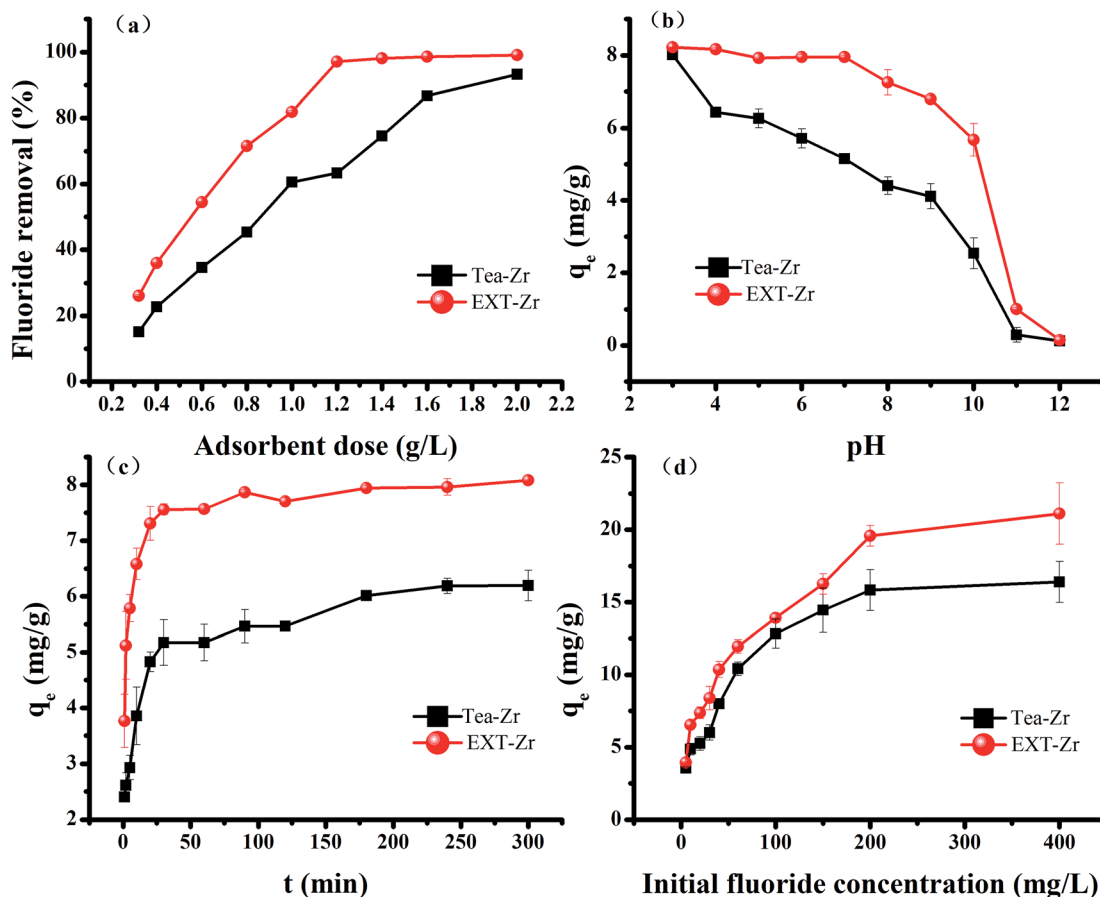
Fig. 3 The effect of adsorbent dose (a), initial pH (b), contact time (c) and initial fluoride concentration (d) on the fluoride adsorption capacity of the tea waste loaded with zirconium (Tea-Zr) and extruded tea loaded with zirconium (EXT-Zr).

tea, Tea-Zr, did not reach equilibrium at 1.2 g L^{-1}, at which point the defluoridation rate was only 61%. The adsorption rate continued to increase with the dose of Tea-Zr. These experimental results showed that EXT-Zr had a better overall adsorption effect. For further experiments, a biosorbent dose was 1.2 g L^{-1} was used to balance cost and effectiveness and to reflect the capacity of the modified tea-based biosorbent.

3.2.2. Effect of solution pH. The effect of pH on fluoride adsorption is displayed in Fig. 3b. The adsorption experiment was carried out for 90 min at a concentration of 10 mg L^{-1}

fluoride, 1.2 g L^{-1} biosorbent and at a pH of 3 to 12. Compared with Tea-Zr, EXT-Zr had a higher adsorption capacity for fluoride across all pH values. In extremely acidic systems, the adsorption capacity was higher because the surface of the biosorbent was positively charged and the electrostatic adsorption increases the adsorption capacity. At a pH value of 5, the amount of fluoride adsorbed decreased slightly. As the pH value was between 3 to 7, the EXT-Zr maintained a high adsorption capacity (q_e), at around 8 mg g^{-1}. The adsorption capacity of EXT-Zr decreases slightly at pH values of 8–10. Most biosorbents

Table 1 The pseudo-first order and pseudo-second order kinetic modeling results for adsorption of fluoride by Tea-Zr and EXT-Zr[a]

Models	Parameters	Description	Tea-Zr	EXT-Zr
The pseudo-first order model $$\log(q_e - q_t) = \log q_e - \frac{K_1}{2.303}$$	K_1 (min^{-1}) q_e (mg g^{-1}) R^2	The rate constant of pseudo-first order model The equilibrium adsorption capacity Correlation coefficient	0.0215 3.96 0.8042	0.0155 1.84 0.8555
The pseudo-second order model $\frac{t}{q_t} = \frac{1}{K_2 q_e^2} + \frac{t}{q_e}$	K_2 (g mg^{-1} min^{-1}) q_e (mg g^{-1}) R^2	The rate constant of pseudo-first order model The equilibrium adsorption capacity Correlation coefficient	0.0235 6.22 0.9977	0.0516 8.07 0.9998

[a] q_t = the amount of fluoride ion adsorbed at time; t = time (min).

Table 2 Langmuir and Freundlich isotherm constants for adsorption of fluoride by Tea-Zr and EXT-Zr biosorbents[a]

Models		Parameters	Description	Tea-Zr	EXT-Zr
Langmuir isotherm $\dfrac{C_e}{q_e} = \dfrac{1}{q^0 b} + \dfrac{C_e}{q^0}$		q^0 (mg g^{-1})	The maximum amount of F$^-$ adsorbed	17.53	20.56
		b (L mg^{-1})	Langmuir binding constant	0.0355	0.0409
		R^2	Correlation coefficient	0.9851	0.9786
Freundlich isomer $\log q_e = \log k + \dfrac{1}{n}\log C_e$		n	The heterogeneity factor	3.5407	4.3573
		k (mg g^{-1})	Freundlich coefficient of adsorption capacity	3.2236	4.9567
		R^2	Correlation coefficient	0.9103	0.9444

[a] C_e = the solution concentration at equilibrium; q_e = adsorption capacity at equilibrium.

remove fluoride by anion exchange between OH$^-$ and F$^-$.[31] The adsorption capacity of Tea-Zr decreases to greater extents than does that of EXT-Zr as the pH of the solution increases. Adsorbents effectively removed fluoride in the pH range of 3–10. This showed that EXT-Zr better adsorbs fluoride across a wider pH range. However, the adsorption capacity of EXT-Zr was extremely low at a pH value of 11–12. With the increase of pH, OH$^-$ may be competing with F$^-$ for Zr binding sites, grabbing adsorption sites on the surface of the biosorbent, resulting in a decrease in the ability to adsorb F$^-$.[16]

3.2.3. Effect of contact time. The effect of contact time on fluoride adsorption is displayed in Fig. 3c. The adsorption experiment was carried out at a pH of 6.8 ± 0.3 and a concentration of 10 mg L^{-1} of fluoride solution for a contact time of 1 to 300 min. The results clearly showed that the adsorption capacity of the biosorbent increases as the reaction time increases. The relationship between the adsorption of fluoride ion and the contact time of Tea-Zr was similar to that of EXT-Zr. However, the adsorption effect of EXT-Zr was much better than that of Tea-Zr. Tea-Zr never absorbed as much fluoride even after 300 min. EXT-Zr removed more than 90% of the fluoride in the first 30 min, indicating that the biosorbent has enough sites to adsorb fluoride in the early stage of the reaction.[32] The adsorption reached equilibrium at 90 min, thus, 90 min was chosen as the reaction time for the next works.

3.2.4. Effect of initial fluoride concentration. The effect of initial concentration on fluoride adsorption is shown in Fig. 3d. The adsorption experiment was performed with an initial fluoride concentration ranging from 5 to 400 mg L^{-1} at pH 6.8 ± 0.3 and

for 90 min. With the initial fluoride concentration increased, the removal of fluoride capacity of the adsorbent increased. The initial fluoride concentration reached adsorption equilibrium at 200 mg L^{-1}. Adsorption first increased and then reached an equilibrium. This may be caused by the relatively large quantity of active sites within the biosorbent at a low fluoride concentration[32] that become saturated as the initial concentration increases, and the surface active sites gradually reach saturation, so that the adsorption gradually moves towards stability.[33]

3.3. Adsorption kinetics

To explore the theory of fluoride adsorption by zirconium-loaded extruded tea waste, the experimental data was simulated by kinetic models[34] (Table 1, Fig. S1a and b†). The values of K_1, K_2 and q_e were calculated from the slope and intercept. For EXT-Zr, the R^2 value of the pseudo-second order model was 0.9998, larger than the pseudo-first order model (R^2 value of 0.8555). This indicated that the pseudo-second order kinetics model better describes the adsorption action by EXT-Zr. This also demonstrated that the adsorption reaction can be a classified as a chemisorption process.[35,36]

3.4. Adsorption isotherm

The adsorption data were analyzed by the Langmuir and Freundlich isotherms models. The Langmuir isotherm presumes that the adsorption occurs in a single-layer on the surface of a homogeneous biosorbent.[37] Whereas the Freundlich adsorption isotherm presumes that the adsorption is

Table 3 Maximum adsorption value of EXT-Zr and other adsorbent materials on fluoride

Adsorbent	q^0 (mg g^{-1})	pH	Contact time (min)	Reference
AC-Zr	5.400	4	180	8
UTP-Zr	12.43	3–10	120	21
Zr(IV)-GP	7.500	3	60	46
MBC	9.000	2–10	5	6
Fe(III)-ASF	0.400	7	60	47
PA-Fe(III)-ASF	0.200	7	60	47
Oyster shell coated with Al (OH)$_3$	5.844	8.07	240	48
ZCOP	5.605	6	50	49
Ficus benghalensis leaves biosorbent	2.200	7	60	50
Cocos nucifera Linn. root biosorbent	2.000	7	90	51
RSL	15.80	7.94		52
EXT-Zr	20.56	3–10	90	This study

heterogeneous and that the adsorption process is not limited to a single layer, but is a multiphase adsorption process.[38]

The R^2 value (0.9786) of the Langmuir isotherm model for the adsorbent EXT-Zr was higher than that of the Freundlich model (0.9444) (Fig. S1c, d† and Table 2). Similarly, the R^2 value (0.9851) of the Langmuir isotherm model for Tea-Zr was larger than that of the Freundlich model (0.9103). Therefore, the Langmuir model showed a good consistency in predicting the defluoridation by the two adsorbents. The modeling also indicated that the surface properties of the EXT-Zr adsorbent are uniform. The calculated maximum removal fluoride capacity of EXT-Zr was 20.56 mg g^{-1}. Compared with other biosorbent in recent years (Table 3), extruded tea waste has stronger adsorption capacity and can be used as a good biological adsorption material.

3.5. Effect of co-existing ions

The effects of co-existing anions on fluoride adsorption is shown in Fig. S2.† These ions, such as Cl$^-$, SO$_4^{2-}$, NO$_3^-$, or HCO$_3^-$, exist in both wastewater and groundwater, and these ions would be present and probably competing with fluoride in time of the adsorption process. The experimental results displayed that the Cl$^-$ and NO$_3^-$ have insufficient effect on the adsorbent, and the fluoride removal effect was hardly affected, even at 200 mg L^{-1}. The SO$_4^{2-}$ slightly affected the defluoridation process, resulting in a slight decrease in fluoride removal efficiency. The HCO$_3^-$ had a greater impact on the adsorbent, decreasing the fluoride adsorption by EXT-Zr by nearly 50% at the low concentration of 50 mg L^{-1}. This interference may be due to the initial increase in pH caused the significant decrease in fluoride adsorption.[20]

3.6. Characterization of the samples and study of the adsorption mechanism

3.6.1. Characterization of the biosorbent samples. The elemental make-up of the EXT-Zr before and after (EXT-Zr-F) adsorption of fluoride were characterized by EDS (Fig. S3†), respectively. EDS analysis showed the elemental peaks, with

only carbon and oxygen in the EXT (Fig. S3a†). But in EXT-Zr, there was an additional peak, for zirconium, which illustrated that the zirconium was successfully loaded onto the EXT (Fig. S2b†). After fluoride adsorption, another peak appeared for fluoride, which illustrated that the fluoride was successfully adsorbed onto EXT-Zr (Fig. S3c†).

The surface of the EXT-Zr appeared to be very rough in SEM images (Fig. 1d). XRD analysis was performed to further study the structure of Tea and EXT-Zr (Fig. S3d†). In the EXT-Zr sample, there was not a significant aqueous zirconium peak, indicating that the amorphous nature of the EXT adequately supported the zirconium ions and that ions were not freely floating in the solution. Amorphous materials are known to have more active sites on their surfaces, such that they can be used as adsorbents.[33]

3.6.2. FTIR study. In order to better understand the adsorption process of fluoride, it was further analyzed by FTIR (Fig. 4). In the raw tea waste, the peak at 3423.36 cm^{-1} is attributed to the hydrogen bonding of –OH stretching, while the peak of the strong stretching vibration at 1632.63 cm^{-1} and 1437.78 cm^{-1} is attributed to the presence of carboxyl groups.[39] After extrusion, the hydroxyl group was shifted to 3146.98 cm^{-1}, the peak of the carboxyl group was shifted to 1651.80 cm^{-1} and 1451 cm^{-1}, probably due to the effect of water and high temperature during the extrusion process. After loading zirconium, the carboxyl groups shifted to 1636.44 cm^{-1} and 1437.92 cm^{-1}, indicating that zirconium interacts with the carboxyl group.[40] A new peak appears at 433.92 cm^{-1} for Zr–O,[41] and a new peak at 1546.15 cm^{-1} represents Zr–OH.[42] After the fluoride adsorption, the peak of Zr–OH became weak, indicating that the process of removing the fluoride involved the hydroxyl group of the metal oxide.

3.6.3. XPS study. To explore the possible adsorption mechanism underlying fluoride removal, XPS measurements were made, as shown in Fig. 5 and Table S1.† The zirconium peak appeared clearly in the loaded EXT (Fig. 5a and b). The elemental ratio of Zr(IV) in EXT and EXT-Zr were 0 and 6.02%, respectively, indicating that zirconium was successfully loaded
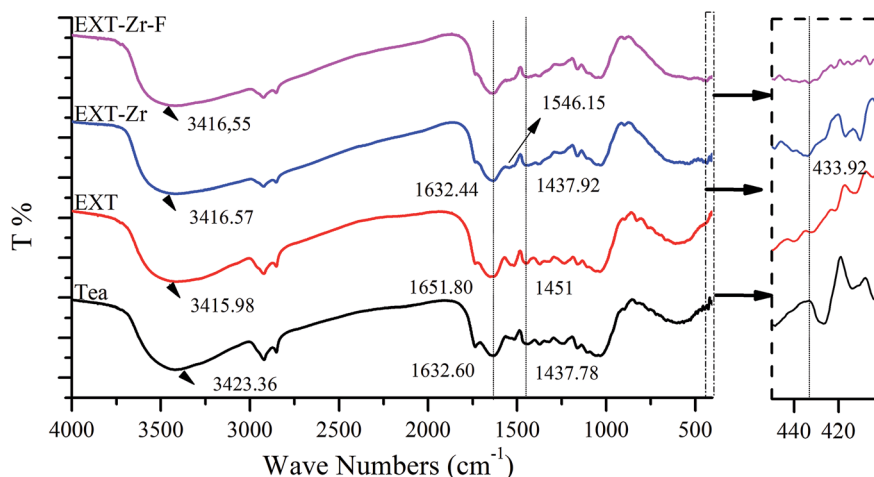

Fig. 4 FTIR spectra of tea, tea waste with zirconium (Tea-Zr), extruded with zirconium before (EXT-Zr) and after (EXT-Zr-F) fluoride adsorption.

onto the EXT. After fluoride adsorption, a peak of fluoride appeared clearly (Fig. 5c), indicating that fluorine was successfully adsorbed. A narrow XPS spectra (194–172) showed that the peak corresponding to the binding energy of Zr 3d before adsorption of fluoride was located at 182.56 eV and after fluoride adsorption shifted to 182.65 eV (Fig. 5d), indicating a change in the zirconium species. Binding with the most

electronegative element, fluoride, results in a decrease in the electron concentration of Zr, which increases the 3d binding energy. At the same time, a peak of fluoride appeared, and the relative content of fluoride on the surface after EXT-Zr adsorption increased to 2%, which showed that fluoride was adsorbed by the adsorbent successfully. In addition, after adsorption the binding energy of the F 1s peak (684.8 eV) was higher than that
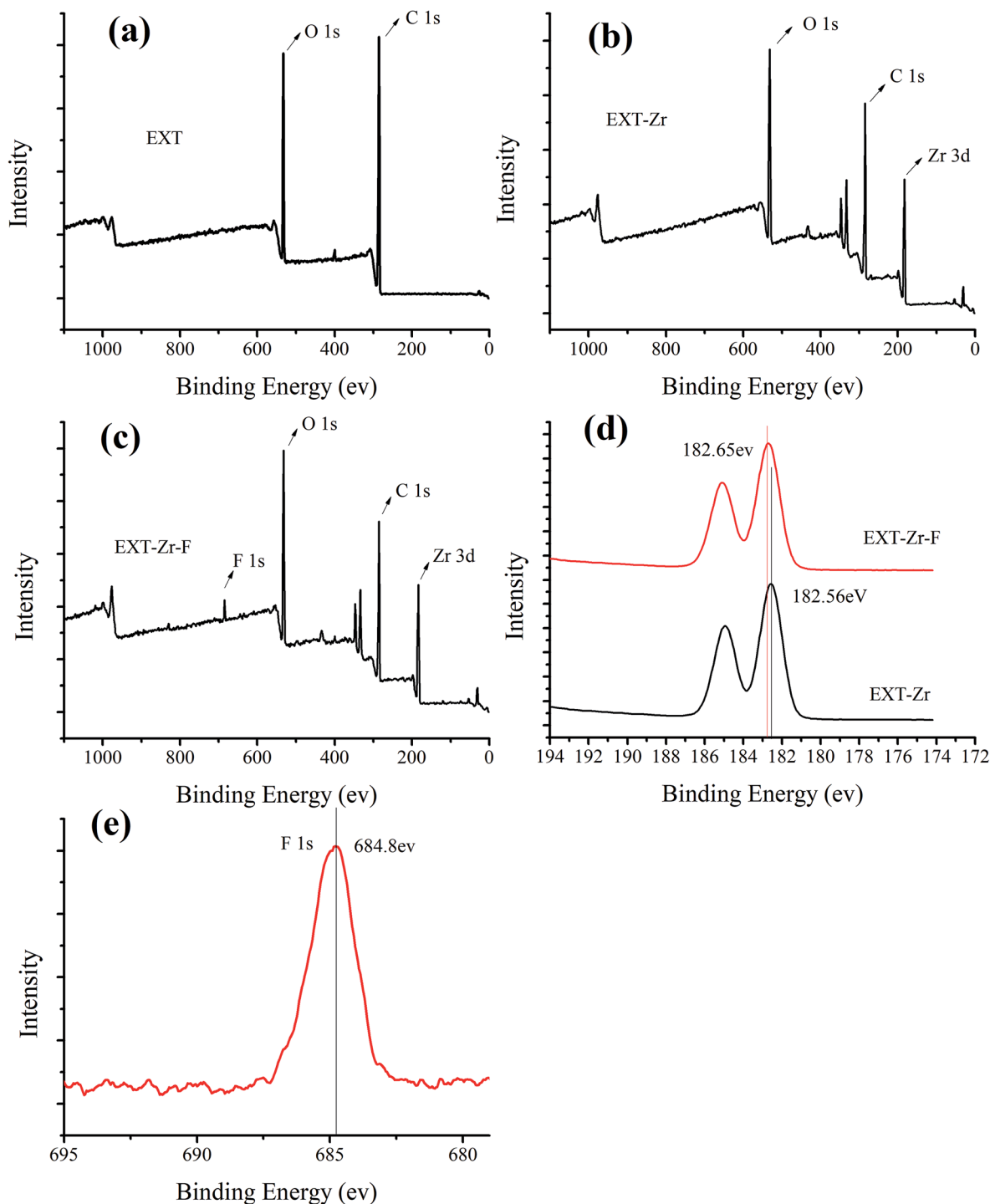
Fig. 5 XPS spectra of extruded tea (EXT), extruded tea with zirconium before (EXT-Zr) and after (EXT-Zr-F) fluoride adsorption. (a–c) Wide scan spectra, (d) Zr 3d and (e) F 1s.
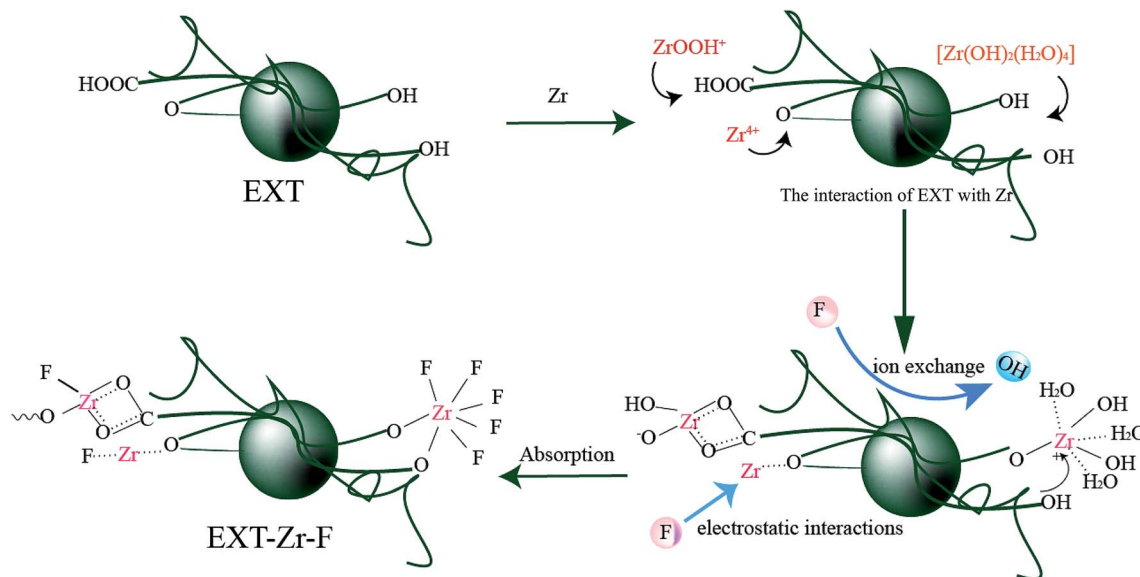
Fig. 6 The proposed mechanism of fluoride adsorption by extruded tea loaded with zirconium (EXT-Zr).

of NaF (684.5 eV) (Fig. 5e), demonstrating that EXT-Zr adsorbed fluoride mainly through chemical adsorption.[43] These results indicated that the fluoride removal process directly involved the Zr and confirmed that the strong interaction between Zr and F had high electronegativity.[44]

The analysis of the extruded tea product and how it adsorbs fluoride allowed for the proposal of the following model. EXT-Zr can form a complex with water through dissociation between the charged surfaces. The adsorption process is mainly through ion exchange, with some electrostatic interactions (Fig. 6).

In a mildly acidic or neutral system the number of sites carrying positive charges on the biosorbent is reduced, some even become negatively charged, resulting in the reduction of the protonation of the hydroxyl. Under these conditions, ion exchange between the hydroxide ion and the fluoride ion mainly occurs.[45]

In an extremely acidic system, the hydroxyl group is protonated and the electrostatic interaction becomes one of the adsorption methods. The surface of the EXT-Zr will be positively charged, which electrostatically attracts the negatively charged F$^-$, thus enhancing fluoride reduction.[21]

4. Conclusion

A novel biosorbent was made by loading zirconium with twin-screw extrusion treatment. Through the extrusion process, the pore size of the tea waste increased to expose more functional groups. Therefore, EXT-Zr had a better adsorption effect than Tea-Zr. EXT-Zr also defluoridated the aqueous solution over a wide pH range. The kinetics model of the adsorption indicates that the process was *via* chemical absorption. The Langmuir isotherm model presented the better fit with high R^2 values and figured out a maximum adsorption capacity of 20.56 mg g^{-1}. These results indicated that the modification of tea waste

through extrusion can improve the adsorption efficiency of a zirconium-loaded biosorbent.

Conflicts of interest

There are no conflicts to declare.

Acknowledgements

References

1 S. Tangsir, L. D. Hafshejani, A. Lähde, M. Maljanen, A. Hooshmand, A. A. Naseri, H. Moazed, J. Jokiniemi and A. Bhatnagar, *Chem. Eng. J.*, 2016, **288**, 198–206.

2 G. Singh, B. Kumari, G. Sinam, N. Kumar and S. Mallick, *Environ. Pollut.*, 2018, **239**, 95–108.

3 S. Aubrey and W. P. T. James, *Public Health Nutr.*, 2014, **17**, 2176–2184.

4 H. J. Gao, Y. Q. Jin and J. L. Wei, *Environ. Monit. Assess.*, 2013, **185**, 3687–3695.

5 X. Fan, D. J. Parker and M. D. Smith, *Water Res.*, 2003, **37**, 4929–4937.

6 N. B. Dewage, A. S. Liyanage, C. U. Pittman Jr, D. Mohan and T. Mlsna, *Bioresour. Technol.*, 2018, **263**, 258.

7 K. K. Yadav, N. Gupta, V. Kumar, S. A. Khan and A. Kumar, *Environ. Int.*, 2018, **111**, 80–108.

8 A. Mullick and S. Neogi, *Ultrason. Sonochem.*, 2018, **45**, 65.

This journal is © The Royal Society of Chemistry 2019

9   S. Dubey, M. Agarwal and A. B. Gupta, *J. Mol. Liq.*, 2018, **266**, 349–360.

10 S. Mukherjee and G. N. Halder, *Environ. Prog. Sustainable Energy*, 2016, **35**, 1305–1316.

11 D. H. Phillips, B. Sen Gupta, S. Mukhopadhyay and A. K. Sen Gupta, *J. Environ. Manage.*, 2018, **215**, 132–142.

12 V. E. dos Anjos, J. R. Rohwedder, S. Cadore, G. Abate and M. T. Grassi, *Appl. Clay Sci.*, 2014, **99**, 289–296.

13 G. Patra, P. Das, S. Chakraborty and B. C. Meikap, *J. Environ. Sci. Health, Part A: Toxic/Hazard. Subst. Environ. Eng.*, 2018, **53**, 1–8.

14 N. M. Zúñigamuro, A. Bonillapetriciolet, D. I. Mendozacastillo, H. E. Reynelávila and J. C. Tapiapicazo, *J. Fluorine Chem.*, 2017, **197**, 63–73.

15 M. Dessalegne, F. Zewge and I. Diaz, *J. Chem. Technol. Biotechnol.*, 2017, **92**, 595–603.

16 S. Raghav and D. Kumar, *Carbohydr. Polym.*, 2019, **203**, 430–440.

17 S. Raghav, S. Nehra and D. Kumar, *J. Mol. Liq.*, 2019, **284**, 203–214.

18 S. Raghav, S. Nehra and D. Kumar, *Process Saf. Environ. Prot.*, 2019, **127**, 211–225.

19 H. Hu, L. Yang, Z. Lin, X. Xiang, X. Jiang and L. Hou, *Int. J. Biol. Macromol.*, 2018, **114**, 256–262.

20 H. M. Cai, G. J. Chen, C. Y. Peng, Z. Z. Zhang, Y. Y. Dong, G. Z. Shang, X. H. Zhu, H. J. Gao and X. C. Wan, *Appl. Surf. Sci.*, 2015, **328**, 34–44.

21 H. Cai, L. Xu, G. Chen, C. Peng, F. Ke, Z. Liu, D. Li, Z. Zhang and X. Wan, *Appl. Surf. Sci.*, 2016, **375**, 74–84.

22 I. S. Ng, X. Wu, X. Yang, Y. Xie, Y. Lu and C. Chen, *Bioresour. Technol.*, 2013, **145**, 297–301.

23 J. Li, M. Thompson and D. J. W. Lawton, *J. Polym. Environ.*, 2019, **27**, 643–651.

24 D. Theng, G. Arbat, M. Delgado-Aguilar, B. Ngo, L. Labonne, P. Mutje and P. Evon, *Eur. J. Wood Wood Prod.*, 2019, **77**, 15–32.

25 A. Duque, P. Manzanares and M. Ballesteros, *Renewable Energy*, 2017, **114**, 1427–1441.

26 C. H. Choi and K. K. Oh, *Bioresour. Technol.*, 2012, **110**, 349–354.

27 F. Berzin, T. Amornsakchai, A. Lemaitre, E. Di Giuseppe and B. Vergnes, *Polym. Compos.*, 2018, **39**, 4115–4122.

28 A. S. A. da Silva, R. S. Sobral Teixeira, T. Endo, E. P. S. Bon and S.-H. Lee, *Green Chem.*, 2013, **15**, 1991–2001.

29 H. Liu, B. Pang, Y. Zhao, J. Lu, Y. Han and H. Wang, *Fuel*, 2018, **221**, 21–27.

30 G. Zhang, Z. He and W. Xu, *Chem. Eng. J.*, 2012, **183**, 315–324.

31 P. Liang, R. An, R. Li and D. Wang, *Int. J. Biol. Macromol.*, 2018, **111**, 255–263.

32 S. Mukherjee, S. Dutta, S. Ray and G. Halder, *Environ. Sci. Pollut. Res.*, 2018, 1–17.

33 L. Xu, G. Chen, C. Peng, H. Qiao, F. Ke, R. Hou, D. Li, H. Cai and X. Wan, *Carbohydr. Polym.*, 2017, **160**, 82–89.

34 K. S. Prasad, Y. Amin and K. Selvaraj, *J. Hazard. Mater.*, 2014, **276**, 232–240.

35 Q. Zhou, X. Lin, B. Li and X. Luo, *Chem. Eng. J.*, 2014, **256**, 306–315.

36 Z. Rahimi, A. A. Zinatizadeh and S. Zinadini, *Environ. Technol.*, 2018, 1–11.

37 M. Rosa, R. Di Felice and S. Corni, *Langmuir*, 2018, **34**, 14749–14756.

38 Z. Yu, C. Xu, K. Yuan, X. Gan, C. Feng, X. Wang, L. Zhu, G. Zhang and D. Xu, *J. Hazard. Mater.*, 2017, **346**, 82–92.

39 H. Cai, G. Chen, C. Peng, L. Xu, Z. Zhang, F. Ke and X. Wan, *RSC Adv.*, 2015, **5**, 101819–101825.

40 J. Wang, L. Wu, J. Li, D. Tang and G. Zhang, *J. Alloys Compd.*, 2018, **753**, 422–432.

41 L. Halla Velazquez-Jimenez, R. H. Hurt, J. Matos and J. Rene Rangel-Mendez, *Environ. Sci. Technol.*, 2014, **48**, 1166–1174.

42 X. Dou, D. Mohan, C. U. Pittman Jr and S. Yang, *Chem. Eng. J.*, 2012, **198**, 236–245.

43 L. Wang, Y. Xie, J. Yang, X. Zhu, Q. Hu, X. Li and Z. Liu, *RSC Adv.*, 2017, **7**, 54291–54305.

44 Y. Jia, B. S. Zhu, K. S. Zhang, Z. Jin, B. Sun, T. Luo, X. Y. Yu, L. T. Kong and J. H. Liu, *Chem. Eng. J.*, 2015, **268**, 325–336.

45 Y. Liu, Q. Fan, S. Wang, Y. Liu, A. Zhou and L. Fan, *Chem. Eng. J.*, 2016, **306**, 174–185.

46 Y. Zhang and K. Huang, *RSC Adv.*, 2019, **9**, 7767–7776.

47 H. T. Mwakabona, H. R. Mlay, B. Van der Bruggen and K. N. Njau, *J. Hazard. Mater.*, 2019, **362**, 99–106.

48 H. Y. H. Chang, Y.-L. Kuo and J. C. Liu, *Sci. Total Environ.*, 2019, **652**, 1331–1338.

49 R. Jha, U. Jha, R. K. Dey, S. Mishra and S. K. Swain, *Desalin. Water Treat.*, 2015, **53**, 2144–2157.

50 A. M. George and A. R. Tembhurkar, *Sustainable Chem. Pharm.*, 2018, **10**, 125–133.

51 A. M. George and A. R. Tembhurkar, *Chin. J. Chem. Eng.*, 2019, **27**, 92–99.

52 T. A. M. Msagati, B. B. Mamba, V. Sivasankar and K. Omine, *Appl. Surf. Sci.*, 2014, **301**, 235–243.